Available online at www.sciencedirect.com
ScienceDirect
Trans. Nonferrous Met. Soc. China 33(2023) 1066−1085
Transactions of Nonferrous Metals Society of China
www.tnmsc.cn

Effect of two-step increased temperature thermal rolling on anisotropy and stretch formability of AZ31 magnesium alloy sheets

Li-fei WANG[1,2,3], Xiao-huan PAN[1], Xing-xiao ZHU[1], Bin XING[2], Hua ZHANG[4], Li-wei LU[5], Hong-xia WANG[1], Wei-li CHENG[1], Maurizio VEDANI[6]

1. Shanxi Key Laboratory of Advanced Magnesium-based Materials, College of Materials Science and Engineering, Taiyuan University of Technology, Taiyuan 030024, China;
2. National Engineering Laboratory for Industrial Big-data Application Technology, Chongqing Innovation Center of Industrial Big-data Co., Ltd., Chongqing 400707, China;
3. School of Materials Science and Engineering, Shanghai Jiao Tong University, Shanghai 200240, China;
4. Institute for Advanced Studies in Precision Materials, Yantai University, Yantai 264005, China;
5. Hunan Provincial Key Laboratory of High Efficiency and Precision Machining of Difficult-to-Cut Material, Hunan University of Science and Technology, Xiangtan 411201, China;
6. Department of Mechanical Engineering, Politecnico di Milano 20156 Milan, Italy

Received 30 November 2021; accepted 12 April 2022

Abstract: The effect of a two-step gradient thermal rolling process on the microstructure evolution and anisotropy as well as the stretch formability of AZ31 magnesium alloys was investigated. Step I was carried out at 300 °C with a small rolling reduction of 15% per pass, while the rolling temperature of Step II was 550 °C with per pass reduction of 40%. Finally, Mg alloy sheets with a thickness of 1 mm were achieved after total four rolling passes. The results indicate that shear bands are generated in rolled samples when the rolling direction is unchanged, while twinning lamellae and recrystallized grains emerge in samples when the rolling direction is changed in Step I. After Step II rolling, the size and amount of shear bands decrease, and grains are refined greatly owing to the enhanced activation of dynamic recrystallization. Besides, non-basal slips, especially prismatic $\langle a \rangle$ slips, are found to be promoted as well based on the in-grain misorientation axis (IGMA) analysis. Therefore, improved mechanical properties, reduced anisotropy, and the improvement of stretch formability of AZ31 Mg alloy sheets are achieved.

Key words: magnesium alloy sheet; two-step increased temperature thermal rolling; non-basal slip; shear band; texture; stretch formability

1 Introduction

As the lightest metal structural material, magnesium alloy has attracted much attentions in the automotive and electronics industries in recent years owing to its low density, excellent specific strength, high specific stiffness and so on [1]. However, only two independent slipping systems can be activated with a strong basal texture [2]. Poor formability would be obtained due to the special close-packed hexagonal (hcp) crystal structure at room temperature [3]. Thus, the application of Mg alloys is limited, and improving the stretch formability is urgent.

ZHAO et al [4] reported that the plasticity of Mg alloys could be enhanced by texture controlling. ZHANG et al [5] fabricated AZ31 alloy sheets via the repeated unidirectional bending (RUB) process and found that the Erichsen value was enhanced

Corresponding author: Li-fei WANG, Tel: +86-18635166011, E-mail: wanglifei@tyut.edu.cn
DOI: 10.1016/S1003-6326(23)66166-7

greatly arising from the decreased basal texture intensity from 30.6 to 8.8. SONG et al [6] developed a new rolling technology by introducing a continuous bending channel into an equal channel angular rolling apparatus. After the ECAR-CB process and annealing, the stretch formability was improved on the texture weakened AZ31 Mg alloy sheets. It was proven that the texture could be modified not only by the induced shear deformation but also by promoting the activation of non-basal slips during deformation. CHINO et al [7] stated that splitting of the basal plane would be generated and the basal texture was weakened greatly after the addition of minor amount of Ce (0.2 wt.%) during rolling due to the promotion of prismatic slips. The stretch formability was improved obviously at room temperature. CHAUDRY et al [8] found the similar phenomenon after adding 0.5 wt.% Ca into AZ31 Mg alloys. During hot rolling, not only basal slips but also prismatic slips were enhanced so that non-basal slips competed with basal slips which resulted in the weakening of the basal texture.

The activation of non-basal slips can also be promoted by the high temperature-induced strain with a higher thermal activation. TROJANOVÁ et al [9] indicated that the critical resolved shear stress (CRSS) of non-basal prismatic slips was reduced obviously at higher deforming temperature on Mg alloys. Thus, their activities were enhanced. HUANG et al [10] reported that the intensity of basal texture on AZ31 Mg alloy sheet was reduced from 15.4 to 2.7 when the finished pass rolling temperature was above 520 °C owing to the activation of non-basal dislocations, while the Erichsen test (IE) value improved at room temperature. However, more literatures about the texture controlling induced by high-temperature strain have not been found. In addition, it is reported that the strain path routes have a significant effect on the texture weakening as well as stretch formability. ZHANG et al [11] revealed that the intensity of the {0002} basal texture was reduced remarkably on AZ31 Mg alloy sheets by three routes rolling at warm temperature. MA et al [12] conducted four routes of asymmetric reduction rolling on AZ31 Mg alloys. The results showed that the strain was more effective when the sheet was rotated by 180° in both RD and ND after the first pass rolling. Therefore, strain path controlling had an important effect on the micro-structure, texture and properties of Mg alloys.

However, the effect of strain path on the texture evolution at higher temperatures has rarely been reported, especially at super-high temperatures. Thus, two-step thermal rolling with limited rolling passes is conducted to investigate the effect of strain path routes on the non-basal slips and texture evolution of Mg alloy in this work. The micro-structure evolutions are compared, and the anisotropy and stretch formability are studied.

2 Experimental

Commercial AZ31 (Mg−3wt.%Al−1wt.%Zn) Mg alloy plates with a thickness of 4 mm were used as the as-received material in this study. Before rolling, all samples were annealed at 350 °C for 1 h. Two-step increased temperature thermal rolling was conducted with different reductions along two strain path routes. To clearly clarify the effect of strain path on the texture evolution at elevated temperatures, Step I rolling was conducted at a temperature of 300 °C with a small strain level (avoiding cracking) of 15% per pass, while the rolling temperature was set as 550 °C in Step II, and a larger rolling reduction of 40% in a single pass was introduced. Finally, the thickness of the Mg alloy plate was reduced to 1 mm after a total of 4 passes rolling. In addition, two routes were applied. Route A is unidirectional rolling, while the direction of Route B changed by 90° per pass. To compare the effect of two-step increased temperature thermal rolling on the stretch formability of Mg alloys, conventional hot rolling was also conducted, especially for the formability measurement. The rolling direction was always along RD, and the temperature was 300 °C with rolling reduction of 15% each pass. After 5 passes, a final sheet with a thickness of 1 mm was obtained. A schematic diagram of the two-step increased temperature thermal rolling is shown in Fig. 1, and the detailed rolling processes are summarized in Table 1. The actual various rolled Mg sheets are shown in Fig. 2. After finishing the rolling, the specimens were annealed at 300 °C for 2 h to obtain a fully uniform recrystallized microstructure.

Then, dog-bone tensile specimens with gauge lengths of 10 mm × 3 mm along RD, 45° and TD were taken from various rolled and annealed Mg alloy sheets. Tensile tests were conducted on

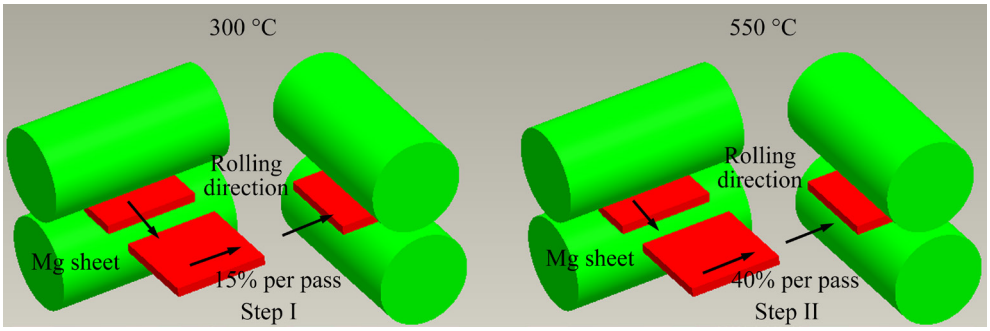

Fig. 1 Schematic diagram of two-step route rolling process

Table 1 Detailed parameters of two-step increased temperature thermal rolling

Route	Step	Pass	Temperature/°C	Direction	Reduction/%	Thickness/mm
A	I	1	300	RD	15	3.40
		2	300	RD	15	2.89
	II	3	550	RD	40	1.73
		4	550	RD	40	1.00
B	I	1	300	RD	15	3.40
		2	300	TD	15	2.89
	II	3	550	RD	40	1.73
		4	550	TD	40	1.00

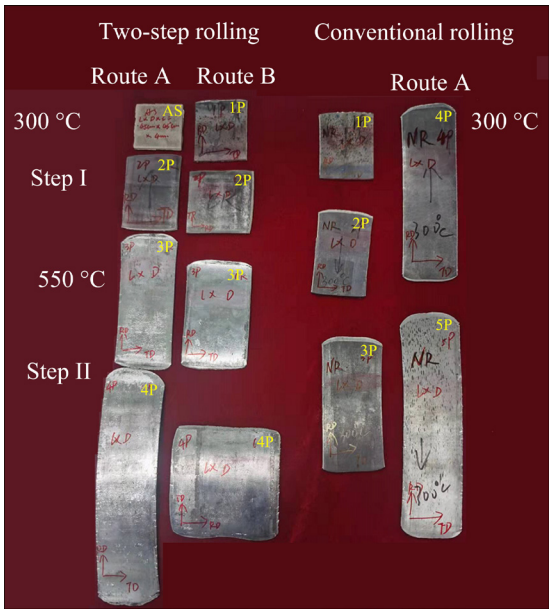

Fig. 2 Actual pictures of AZ31 Mg alloy rolled sheets with various passes

DNS2000 electronic universal testing machine at room temperature. The strain rate was 1×10^{-3} s^{-1}. Each test was repeated three times. The strain hardening coefficient (n-value) was measured from the tensile stress–strain curves. For the Lankford r-value, the samples were stretched to 12%, and then the strain along width and thickness directions was measured. A rectangular sample with a size of 45 mm × 45 mm was used for Erichsen test. The diameter of the hemispherical punch was (20±0.05) mm. The press speed of the punch was 10 mm/min, and the blank force was 10 kN. Engine oil was used as the lubricant at the center of the specimen.

The microstructures before and after annealing were observed with an optical microscopy (OM; Leica DM2700 M). The {0002} pole figures and crystal structure evolution were measured by electron backscatter diffraction (EBSD) analysis using an HKL Chanel 5 System equipped in a scanning electron microscope (JEOL GSM−7800F FEG SEM). Sample preparation for EBSD observation included mechanical grinding and surface polishing. Thereafter, electropolishing was carried out with commercial AC2 solution at a temperature of −20 °C using a voltage of 20 V for 90 s.

3 Results and discussion

3.1 Microstructure evolution

The optical microstructure, inverse pole figure (IPF), grain size distribution, misorientation

distribution map and {0002}, {$10\bar{1}0$}, {$11\bar{2}0$} pole figures of the as-received AZ31 magnesium plate are shown in Fig. 3. It can be seen clearly that equiaxed grains without twins are distributed in the microstructure. The average grain size is approximately 26.4 μm and the average misorientation distribution value is about 34.1°. This means that the microstructure is completely recrystallized. From the IPF map in Fig. 3(b), most grains express a red color, which indicates that most grains lay on the {0002} basal plane. Thus, the *c*-axis of grains is parallel to the normal direction (ND) of the plate, and a typical basal texture is exhibited, although some grains tilt to the transverse direction (TD), as shown in Fig. 3(c). The intensity of the basal texture is 14.23. KUANG et al [13] stated that non-basal slips could not be activated at room temperature owing to larger CRSS. LI et al [14] suggested that basal ⟨*a*⟩ slips would be restrained on Mg alloys in subsequent deformation with a strong basal texture. A smaller Schmid factor (SF) of basal slips can be obtained, which is not conducive to improving the ductility of Mg alloys.

The optical microstructures of various rolled AZ31 Mg alloys on RD−ND plane are shown in Fig. 4. The samples after 1, 2, 3, and 4 passes rolling under Route A and B are namely A1−A4 and B1−B4, respectively, which is consistent with Table 1. Twinning lamellae are generated after one-pass unidirectional rolling along RD, and the grain size does not change much, which is almost similar to as-received specimen. However, shear bands appear as dark sharp straight lines, as shown

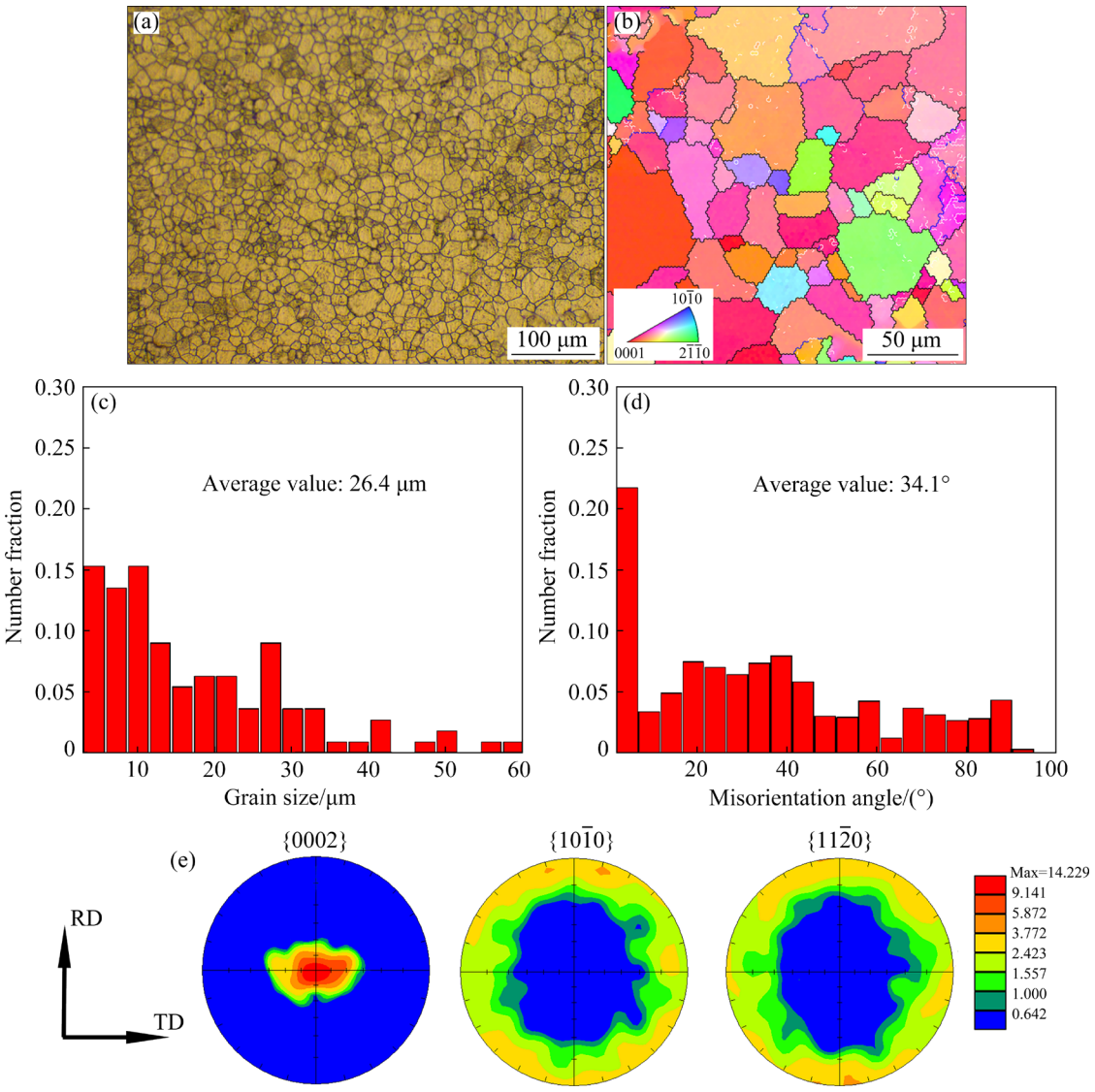

Fig. 3 Microstructure and pole figure of as-received AZ31 magnesium alloys: (a) Optical microstructure; (b) Inverse pole figure (IPF) map; (c) Grain size distribution; (d) Misorientation angle distribution; (e) Pole figures

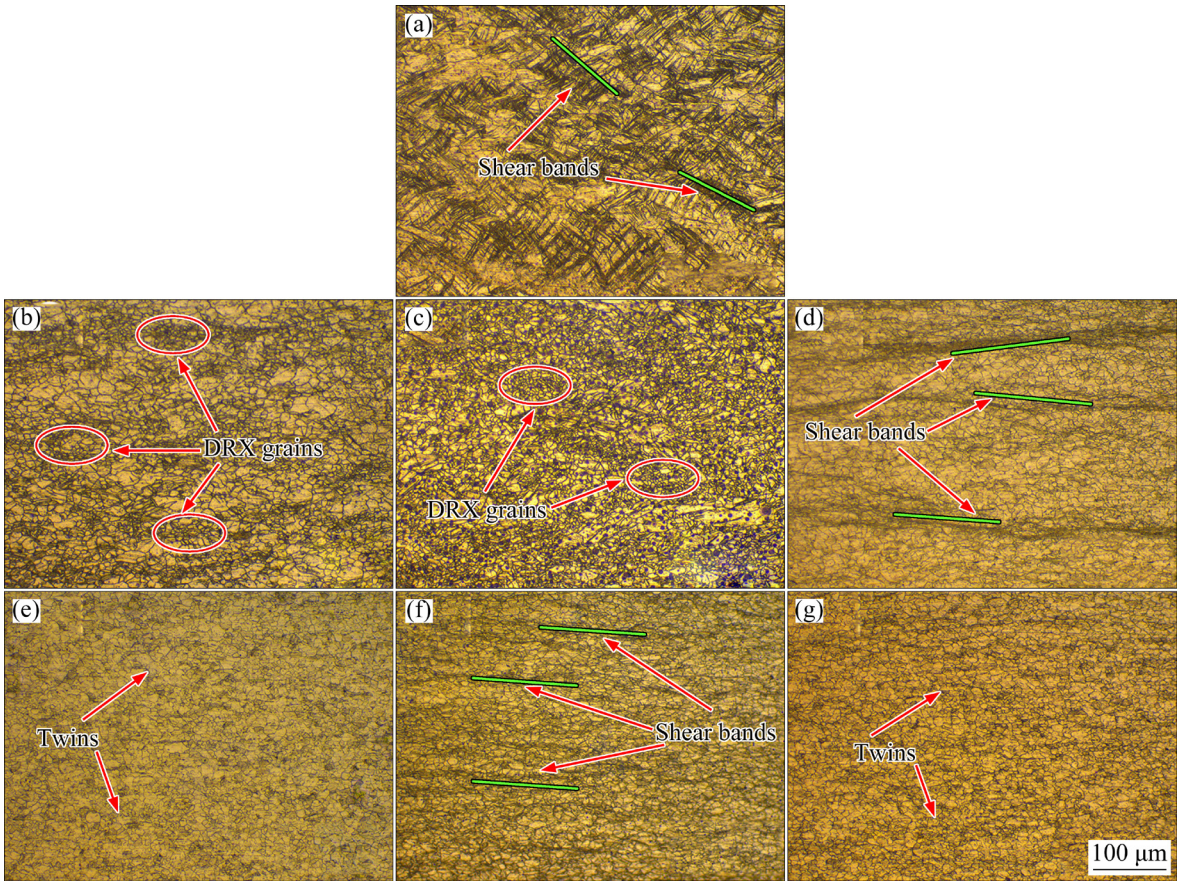

Fig. 4 Optical microstructures of various two-step thermally-rolled AZ31 magnesium alloys without annealing: (a) Sample A1; (b) Sample A2; (c) Sample B2; (d) Sample A3; (e) Sample B3; (f) Sample A4; (g) Sample B4

by red arrows along the blue lines. During the second thermal pass rolling in Samples A2 and B2, it is noted that the deformation is still dominated by twinning. Many twins are distributed in the microstructure. In addition, some new dynamically-recrystallized (DRXed) grains appear, as shown by the red circles in Figs. 4(b, c). In Sample A2, most small new grains are close to the shear bands during unidirectional rolling, which is parallel to RD. However, the distribution of DRXed grains is more uniform, and the volume fraction increases with the rolling direction changing in Sample B2. ZHI et al [15] indicated that the direction of the tensile and compressive stresses on the sheet were always the same during the unidirectional rolling, while it would change continuously when the direction was altered. The changing direction of rolling strain is more likely to lead to grain breakage and larger distortion energy, which favors DRX nucleation. Thus, more DRXed grains are generated in Sample B2.

GUO et al [16] suggested that dislocations accumulated at shear bands during rolling on AZ31 Mg alloys so that the nucleation of DRX behavior would be promoted. Shear band-induced DRX behavior may also start in Sample A2. During the thermal rolling in Step II with a larger reduction of 40% at 550 °C in Sample A3, shear bands and twinning are generated again, as shown in Fig. 3(d). The size of the shear bands becomes narrow and the amount decreases. However, only twinning lamellae emerge when the rolling direction is changed in Sample B3. After the fourth pass rolling, the grain size of two samples is reduced obviously. Shear bands still emerge, but the width in Sample A4 is reduced continuously compared to that in Sample A3. In Sample B4, twins are distributed fully. The evolution of shear bands and twins during the two-step thermal rolling may be related to the enhanced non-basal slip and DRX behaviors with different stress states at elevated temperatures. To clarify the microstructure evolution mechanisms, EBSD analysis was conducted on as-rolled samples, A3 and B3.

IPF maps and {0002} pole figures of the as-rolled A3 and B3 samples without annealing are shown in Fig. 5. The microstructure characteristics are consistent with optical results. The shear bands are obviously acquired in the band map in Sample A3. However, it is difficult to index local crystals inside shear bands, which is probably due to the localized strain concentration. Only some parental grains and larger twinning lamellae are observed. In Sample B3, shear bands cannot be found, and twins

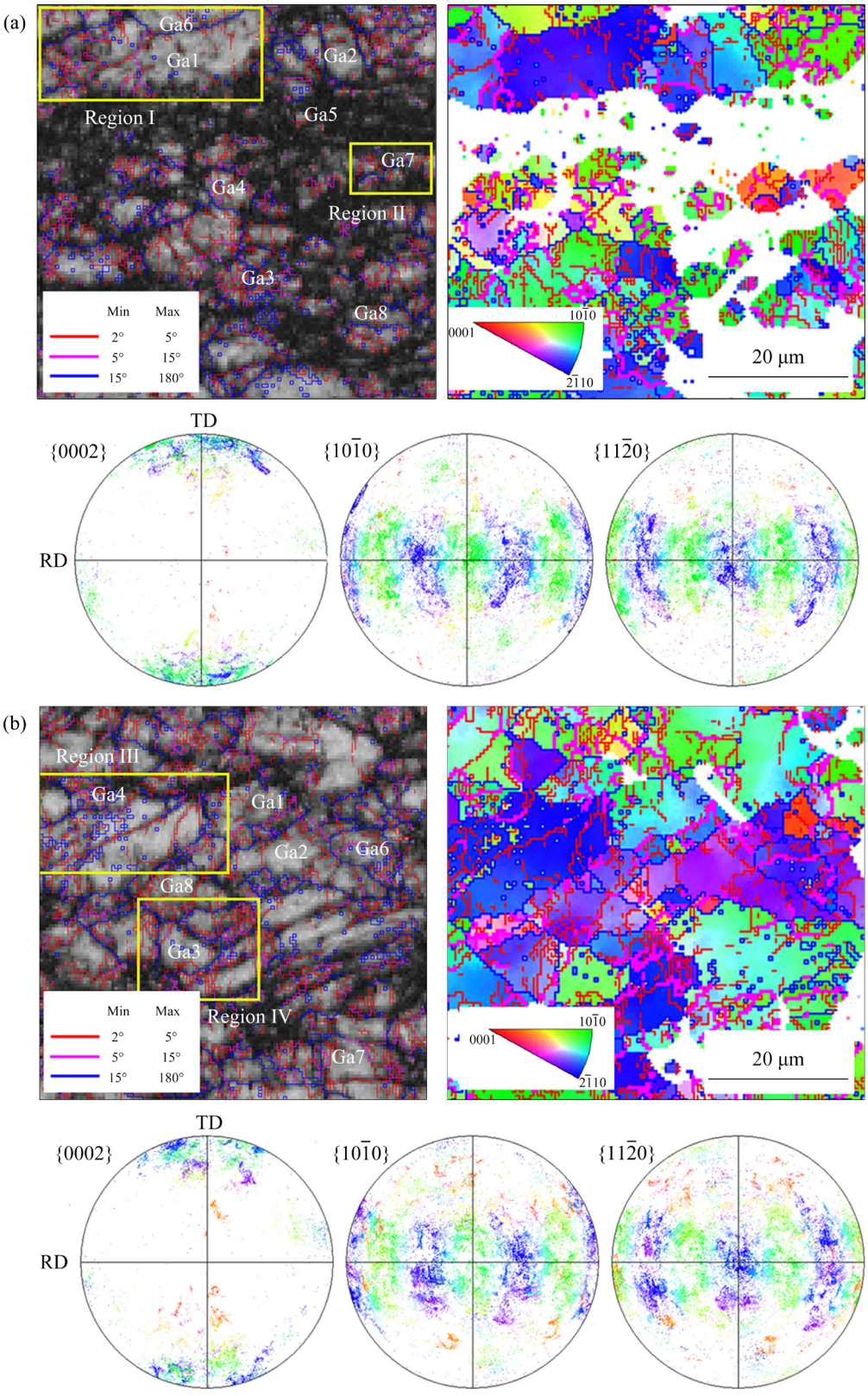

Fig. 5 EBSD maps and pole figures of various rolled samples without annealing: (a) Sample A3; (b) Sample B3

are distributed, which is similar to microstructure in Fig. 4(e). In both samples, large amounts of low angle grain boundaries (LAGBs) are generated, especially 2°−5°, which indicates that most grains are deformed seriously. The *c*-axis of indexed grains in Samples A3 and B3 is rotated from ND to RD, which expresses a blue color compared with that of the as-received sample. In addition, many grains are distributed randomly in the middle part of the {0002} pole, and the fraction is much greater in Sample B3 than in Sample A3. From the $\{11\bar{2}0\}$ and $\{10\bar{1}0\}$ pole figures, more non-basal prismatic grains are expressed in Sample B3. As well known, the orientation of grains is generated mainly related to the deformation mechanism. The grains with a basal orientation are induced due to the activated basal slips, while non-basal orientation grains are induced by non-basal slips, including $\{10\bar{1}0\}$, $\{11\bar{2}0\}$ prismatic $\langle a\rangle$ slips and $\{10\bar{1}1\}$, $\{11\bar{2}1\}$, $\{11\bar{2}2\}$ pyramidal $\langle a+c\rangle$ slips.

To study the detailed deformation mechanisms, in-grain misorientation axis (IGMA) analysis was performed. The IGMA method was first introduced by CHUN et al [17,18]. Based on the tilted Taylor axis of $\langle 0\bar{1}10\rangle$, $\langle 0001\rangle$ and $\langle 1\bar{1}00\rangle$, the $\{0002\}\langle 11\bar{2}0\rangle$ basal slip, $\{10\bar{1}0\}\langle 11\bar{2}0\rangle$ prismatic slip and $\{11\bar{2}2\}\langle 11\bar{2}\bar{3}\rangle$ pyramidal slip can be determined. According to the IGMA method, eight grains are selected randomly in each sample. The misorientation angle concerned in this work ranges from 1.2° to 2.0°. Figure 6 shows the IGMA distributions of various grains in Samples A3 and B3. The grains are marked as Ga1−Ga8 in Sample A3 and Gb1−Gb8 in Sample B3, as shown in Fig. 5. To clarify the texture distribution, the maximum legend of texture intensity is set as 3. The IGMA distributions are mainly concentrated around $\langle uvt0\rangle$ directions in Ga1, Ga2, Ga6, and Ga7. In addition, the maximum intensity is larger than 2, which is considered to have preferential IGMA. According to previous report, $\langle uvt0\rangle$ type rotation is caused owing to the activation of $\langle a\rangle$ type basal and $\langle c+a\rangle$ type pyramidal slips. However, the approximately $\langle 0001\rangle$ rotation is only caused by the activation of prismatic $\langle a\rangle$ slips. It has been reported that the CRSS of basal slips is insensitive to increased temperatures; however, it reduces gradually on non-basal slips when the temperature increases. HAGIHARA et al [19] indicated that the CRSS of non-basal slips showed a strong temperature dependence, which decreased rapidly at approximately 400 °C on Mg89Zn4Y7 alloys. TAKAGI et al [20] stated that the localized prismatic slips were suppressed by the interaction with co-operative basal slips at the transition temperature of 300 °C; however, it was distributed homogenously concurrent with basal slips on the basal plane obove the critical temperature on Mg−Zn−Y single crystal. Both prismatic and basal slips were promoted at elevated temperatures. The CRSS values were relatively similar. Then, the trend continued to reduce as the temperature increased to 450 °C during compression on pure Mg single crystals, as indicated by HAPUIS and

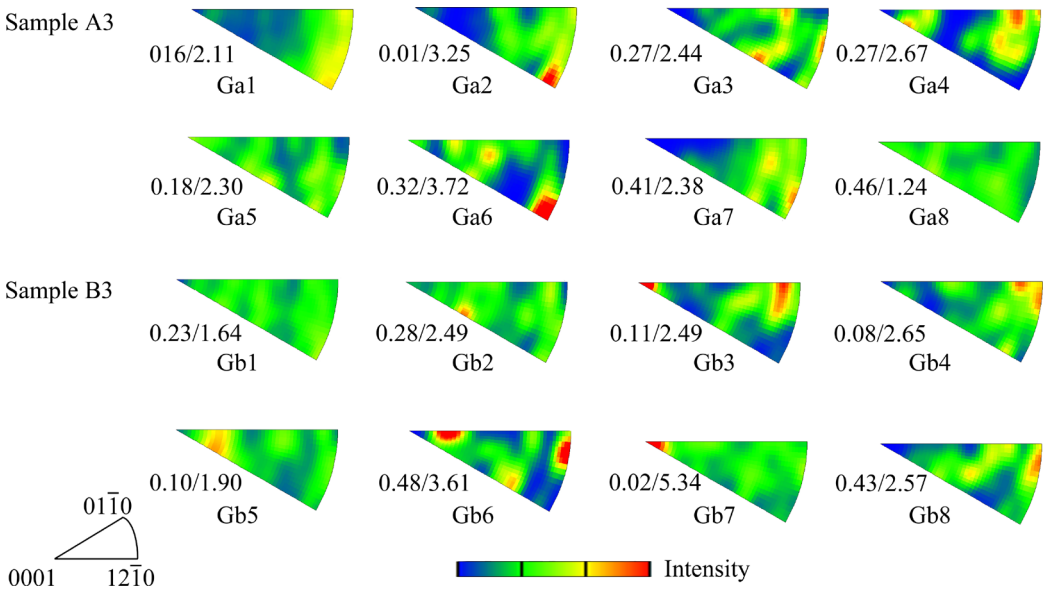

Fig. 6 IGMA distributions of numbered grains in Samples A3 and B3 without annealing in Figs. 5(a, b)

DRIVER [21]. Therefore, in Ga1, Ga2, Ga6, and Ga7, both basal ⟨*a*⟩ slips and pyramidal ⟨*a*+*c*⟩ slips may be activated during rolling at 550 °C. In Ga3, Ga4, and Ga5, the maximum intensity of IGMA tends to rotate along ⟨0001⟩ axis, which means that ⟨*a*⟩ type prismatic slips are also favorable during rolling deformation.

In Sample B3, a preferential IGMA is also emerged in selected grains. However, the IGMA distributions are mainly concentrated around the ⟨0001⟩ axis in Gb3 and Gb7 specifically. Considering that the CRSS of prismatic ⟨*a*⟩ slips is relatively similar to basal slips on Mg alloys above 400 °C, prismatic ⟨*a*⟩ slips should be much easily activated in Gb3 and Gb7. The maximum intensities of IGMA are 10.73 and 5.34 and are located at approximately ⟨0001⟩, which suggests that the deformation is dominated by prismatic ⟨*a*⟩ slips in Gb3 and Gb7. In Gb2, Gb5 and Gb6, the maximum intensity of IGMA tends to approximately the ⟨0001⟩ axis, which also suggests prismatic ⟨*a*⟩ slips are favorable during rolling deformation. In Gb4 and Gb8, the IGMA distributions are concentrated around ⟨*uvt*0⟩, which is mainly caused due to the basal ⟨*a*⟩ slips and pyramidal slips. In Ga8 and Gb1, the intensity is less than 2, which expresses a uniform IGMA. This can be attributed to the coactivation of various slip modes.

Local lattice orientation maps of selected grains in subregions in Fig. 5 are shown in Figs. 7 and 8. The misorientation angle relationship along the line inside and across the grain boundaries are also exhibited. Coarse grains G1−G7 and fine grains G8−G14 close to shear bands are selected to analyze the deformation mechanisms. Grains G1−G7 distribute randomly away from the center of the pole figure. Large amount of LAGBs are presented inside or around the grains, which means that these grains are severely deformed and might not be recrystallized. The line profiles of the point-to-origin along Line 1 in G2 are demonstrated in Fig. 7(a), which indicates that the misorientation angles increase gradually and the peak angle is approximately 13°. This means that a great dislocation activity occurs in G1. Meanwhile, the nearby smaller grains G5 and G6 are distributed

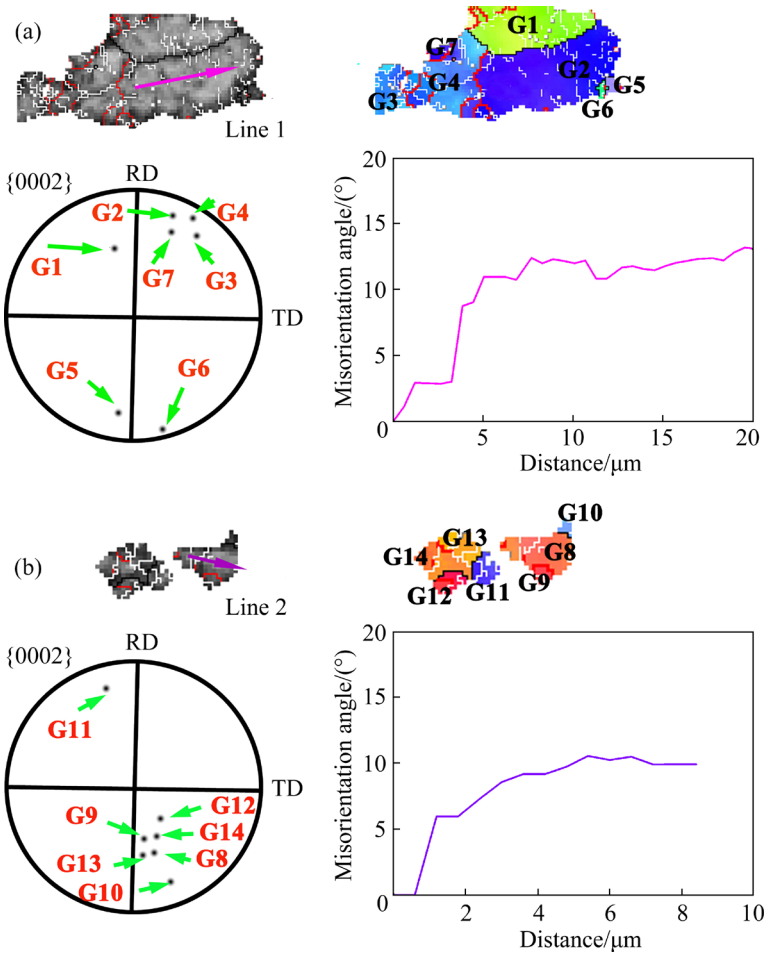

Fig. 7 Local lattice orientation of grains and misorientation angle distribution along Lines 1 (a) and 2 (b) in Sample A3

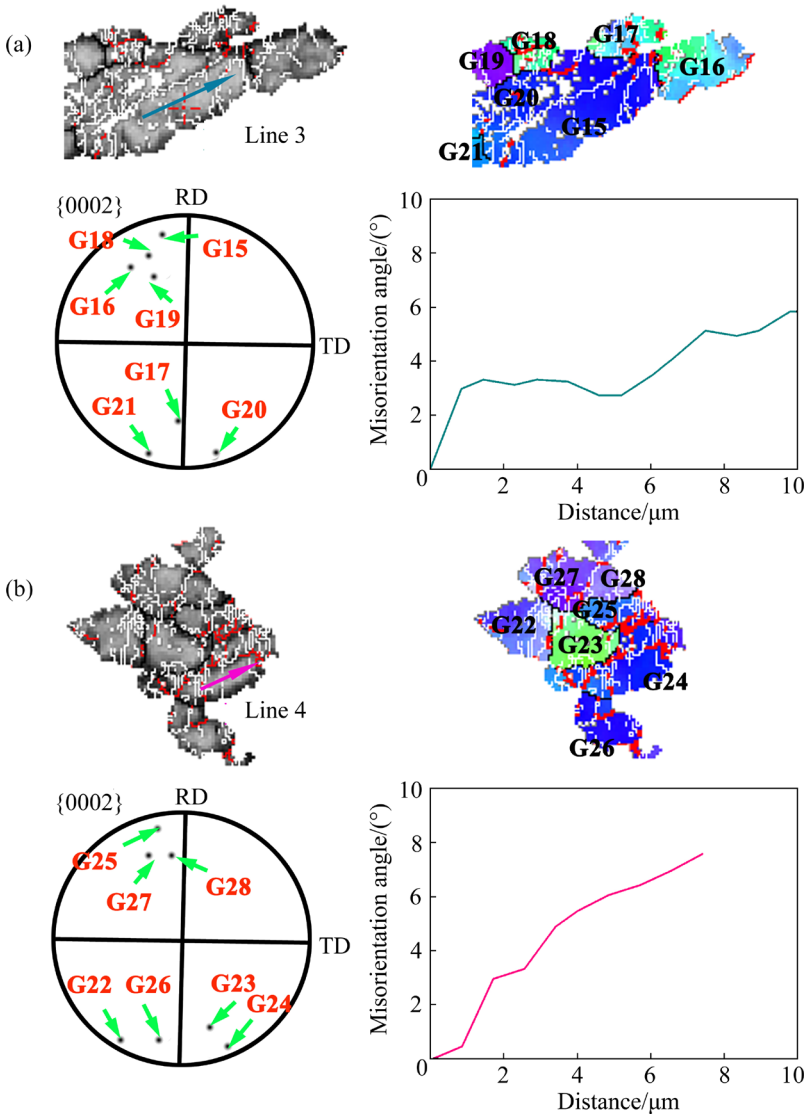

Fig. 8 Local lattice orientation of grains and misorientation angle distribution along Lines 3 (a) and 4 (b) in Sample B3

close to RD, which expresses a non-basal orientation. This is the evidence of CDRX [22]. In addition, the CDRX is proceeded by the non-basal ⟨*a*⟩ slips. It is similar in the fine grain G8 which is close to the shear bands. The misorientation profile along Line 4 increases and the angle exceeds 10°. This indicates that large amounts of dislocations are piled up around shear bands as well as grains. The dislocation density decreases as well when finer grains are formed, as indicated by the misorientation in G8.

In Sample B3, Regions III and IV are selected to analyze the local grain orientation. G15−G28 are detected in two regions, and the distributions are illustrated in the basal pole. It can be seen that grains are distributed away from the center of the pole. Along Lines 3 and 4, the misorientation angle increases; however, the peak value is much lower, which means that the dislocation density is smaller than that in Sample A3. In addition, grains G15−G28 express more random distributions than grains G1−G14. This indicates that the stress concentration is released obviously during Route B rolling due to the enhanced activity of non-basal slips. Thus, in the Step II increased temperature thermal rolling, the deformation activities are enhanced in both samples. As shown in Fig. 5, some grains are distributed randomly in the {0002} pole except for RD-closed twins, especially in Sample B3, and the amount of these grains is much larger. CHO et al [23] reported that the frictional force and compressed force are applied on the sheet during unidirectional rolling. The resultant forces lead to the strain direction tilting from RD to ND,

so that the large flow local dislocations are piled up. ZHANG et al [24] indicated that the generation of shear bands in Mg alloys was associated with deformation twins or dynamic recrystallization near grain boundaries. This high dislocation density contributes to the formation of shear bands. However, due to the enhanced non-basal slips, the stress concentration is released gradually during hot deformation; therefore, the amount of shear bands in Sample A3 is reduced.

Along Route B, the orientation of grains diverges, which favors basal and non-basal slips so that the dislocation piles are prevented and the stress concentration is released much easily. Therefore, only twinning lamellae and DRXed grains emerge in Sample B3. In addition, the generation of shear bands in Sample A3 seems to be related to the DRX behavior at this high rolling temperature, by combining Fig. 6(a) and Fig. 5(d). However, there may be a similar reason in Step I rolling. The rolling temperature is much lower so that basal slips mainly dominate the deformation in both rolled Samples A and B. Due to the pilled dislocations, the shear bands are generated more in Samples A1 and A2, and the twinning is mainly response for the formation of shear bands. However, the dislocation pile-up is much weaker when the rolling direction changes. Thus, there are limited distributions in Sample B2.

The IPF maps, misorientation and grain size distribution of various thermally-rolled Mg sheets after annealing are shown in Fig. 9. All twins and shear bands of the two-step rolled Mg sheets disappear after annealing at 300 °C for 1 h. Equiaxed and red-colored grains are distributed in the microstructure, which means that deformed structures are recrystallized and the grain orientation rotates from RD to ND. The grain sizes are 23.3, 17.4, 15.8, 11.9 and 8.5 μm in Samples A1, A2, B2, A4 and B4, respectively. As the rolling pass increases, grains are refined more obviously, especially at Step II in Samples A4 and B4. JIA et al [25] reported that the temperature played a significant role in the microstructure during rolling of Mg alloys. MA et al [12] indicated that the rolling route influenced the dynamic recovery, which affected the recrystallization behavior of AZ31 Mg alloys. In Step I, by comparing the microstructures with as-received ones, for Sample A1 without annealing and after annealing, the grain size is refined to a small level, as shown in Fig. 7(a). The large amount of twins and shear bands are consumed during the annealing process. However, the faction of the low-angle grain boundaries (LAGB, 0°−15°) is relatively higher, and the average misorientation is approximately 31.1°. After 2 passes rolling with 15% strain at 300 °C, grains are refined more in both routes of rolled samples; in addition, the fraction of LAGBs decreases, and that of the high angle grain boundary (HAGB) increases. Especially by changing the rolling direction in Sample B2, the average misorientation angle is 39.2° compared to Sample A2 with the value of 38.1°.

The phenomenon is similar in the increased temperature Step II rolling process at 550 °C in Samples A4 and B4. The grain size is refined more when the rolling route is changed, and the average misorientation values are 37.8° and 43.2°, respectively, as shown in Figs. 9(d, e), which means that recrystallization behavior is promoted more through rolling Route B. As indicated in as-rolled microstructure without annealing, shear bands always emerge in rolled samples in Route A; however, there are mainly twins in Sample B due to the alternatively changing stress direction. It has been reported that recrystallization nucleation sites are always favored at shear bands [26], twins [27], and intersections between grain boundaries and twins [28]. When increasing the temperature to 550 °C in Step II rolling, thermal activities are promoted, and shear bands are restricted owing to the release of the stress concentration. Although twins are not favored at high temperature, twinning lamellae still exist fully in the rolled microstructures induced by the local large strain of 40%. Thus, static recrystallization occurs easily, and finer grains are formed after the annealing process, as shown in Samples A4 and B4 in Fig. 9. Due to the changing in stress directions, the static recrystallization is significant, and the grains are finer. The peak misorientation of Sample B4 is approximately 40°.

3.2 Texture and Schmid factor

Figure 10 shows the {0002}, $\{10\bar{1}0\}$ and $\{11\bar{2}0\}$ pole figures of the two-step increased-temperature thermal-rolled Mg alloy sheets. All samples still express the characteristics of rolled basal texture; however, the *c*-axis of some grains

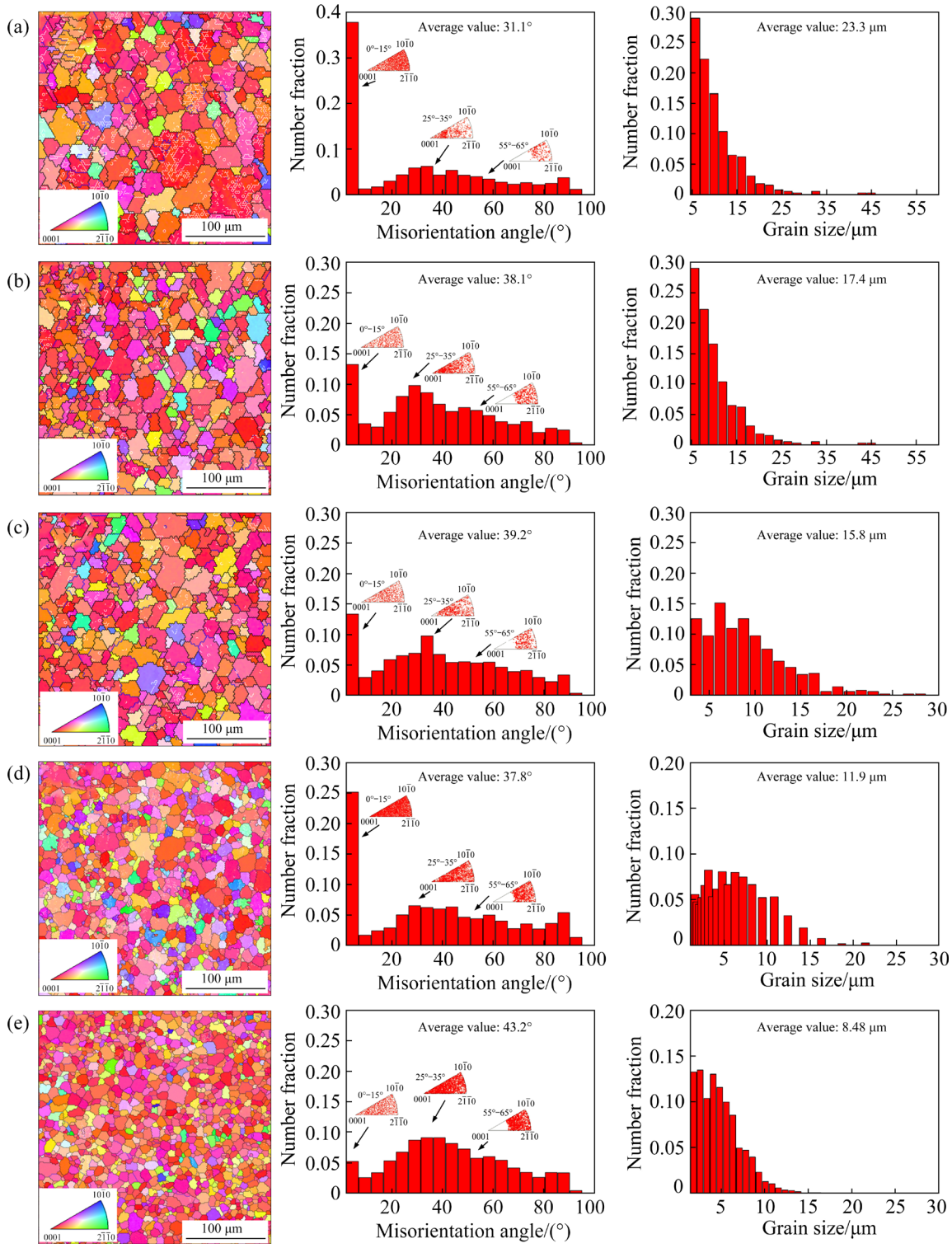

Fig. 9 IPF maps, misorientation distribution and grain size distribution of various thermally-rolled AZ31 Mg alloy plates after annealing: (a) Sample A1; (b) Sample A2; (c) Sample B2; (d) Sample A4; (e) Sample B4

tilts away from ND towards RD and lays on ND-RD plane. With the increase of rolling pass, the intensity of basal texture is reduced gradually to 15.6 (Sample A1), 8.1 (Sample A2), 6.9 (Sample B2), 6.2 (Sample A4), and 5.5 (Sample B4). The weakening of basal texture can be related to the activation of non-basal slip systems. After 1 pass undirectional rolling in Sample A1 with a smaller strain level of 15% at 300 °C, the intensity of the basal texture is strengthened slightly. This may be

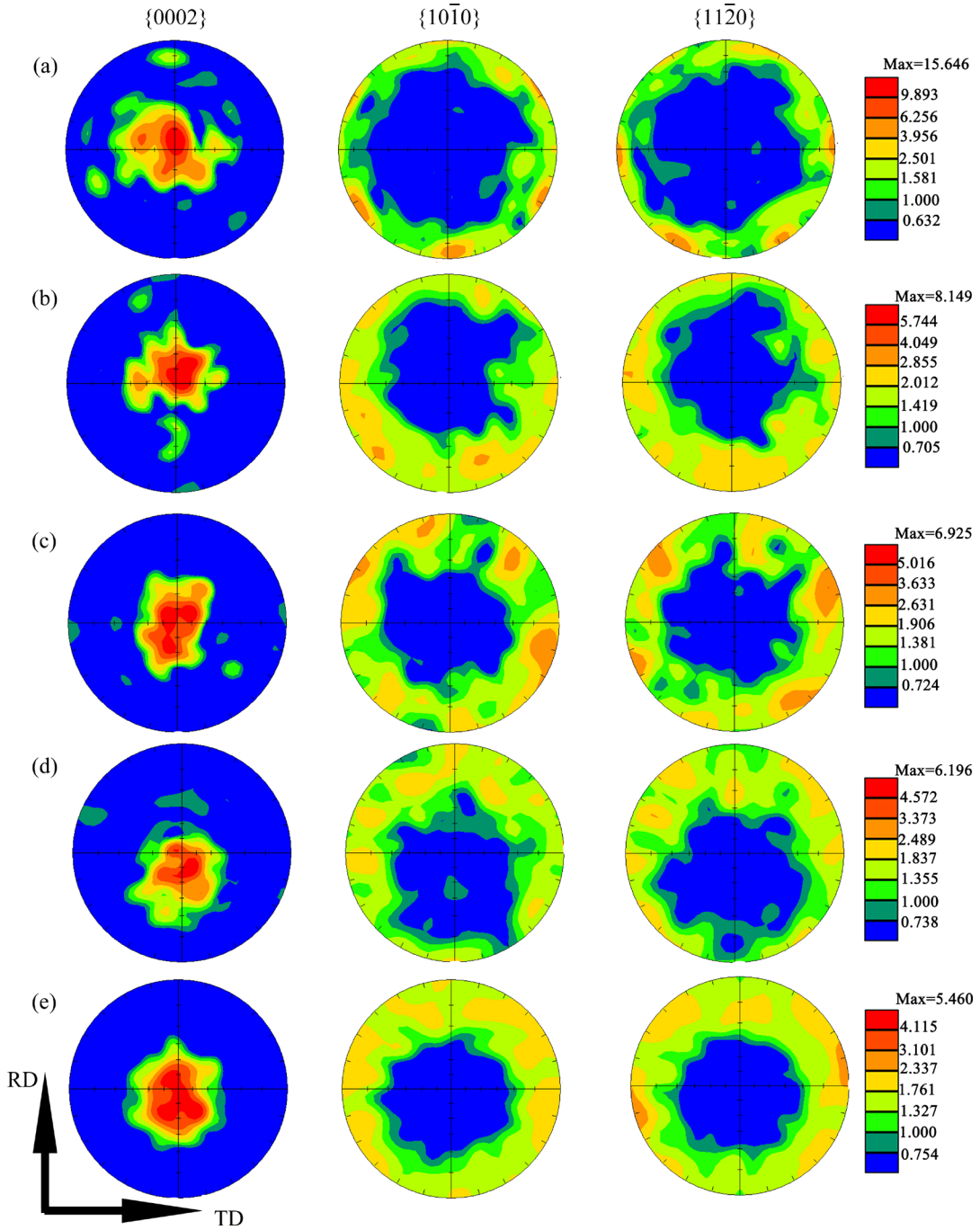

Fig. 10 {0002}, {10$\bar{1}$0} and {11$\bar{2}$0} pole figures of various thermally-rolled AZ31 Mg alloy plates after annealing: (a) Sample A1; (b) Sample A2; (c) Sample B2; (d) Sample A4; (e) Sample B4

due to the induced large amount of shear bands with a high strain concentration. SAMMAN and GOTTSTEIN [29] reported that the inhomogeneous deformation, such as shear bands, would result in a relatively small strain accommodation, which was beneficial to stretching of the basal texture at relatively low temperatures. However, as the rolling processes continue, the number of shear bands decreases. Non-basal slips, recrystallization and stress states may respond to the texture evolution. As shown in Figs. 10(b, c), the basal texture weakens remarkably compared with the as-received and Sample A1 after anealing. In addition, some grains tilt to RD, and the {0002} pole tends to be more divergent, especially in Sample B2. SU et al [30] and ZENG et al [31] indicated that a significant texture weakening occurred due to static recrystallization (SRX) at the pre-existing twins and

grain boundaries. The orientation of new SRXed grains is dependent on the type of twins, as reported by HUANG et al [32].

According to as-rolled samples, A3 and B3, some tensile twinning orientation is distributed in the {0002} pole close to RD, namely, $(10\bar{1}2)$ tensile twins. Therefore, the RD-tilted weakening basal textures are achieved in various thermally-rolled samples. In addition, FLYNN et al [33], and PRASAD and RAO [34] indicated that the primatic $\langle a \rangle$ slips would start above 175 °C, while pyramidal $\langle a+c \rangle$ slips would take out above 225 °C. Thus, non-basal slips compete with basal slips, which does not benefit the formation of basal texture component. As the rolling process proceeds, the density of non-basal slip increases, which promotes the statically-recrystallized (SRXed) grains to nucleate toward various directions, and the basal texture is weakened. However, compared with Sample A2, the intensity of the basal texture is weakened more obviously in Sample B2. This is due to the alternatively changing direction of tensile and compressive stress, which results in more divergence of grain orientation. However, the texture weakening is more significant in Step II increased-temperature rolling with a larger strain degree of 40% each pass at 550 °C. HUANG et al [35,36] indicated that higher temperature deformation would increase the orientation gradients near the grain boundary due to GBS or enhanced non-basal slips. Then, SRX behaviors are likely to start at grain boundaries with larger orientation gradients and higher local dislocation densities. Therefore, a remarkably weakened basal texture is obtained in Samples A4 and B4. The texture weakening effect is more significant with changing the rolling direction at higher temperatures, as shown in Sample B4. A smaller double-peak RD-tilted basal texture almost emerges in the {0002} pole. In addition, HUANG et al [10] also reported that a slight double-peak non-basal texture on AZ31 Mg alloy sheets was generated due to the enhanced non-basal slips during higher temperature rolling. However, it is observed in changed route rolling rather than unidirection rolling in this study, which means that non-basal slips are promoted more when the rolling stress directions are changed alternatively. ZHANG et al [37] reported that the orientation of grains was related to the final rolling route. The tilted direction of grains follows the final rolling direction. However, the orientation of grains is still close to RD, which indicates that the enhanced non-basal slip activities play a more important role than the stress state during high-temperature rolling.

The Schmid factors (SF) of basal slip $\{0001\}\langle 11\bar{2}0\rangle$, prismatic slip $\{10\bar{1}0\}\langle 11\bar{2}0\rangle$, pyramidal slip $\{10\bar{1}1\}\langle 11\bar{2}0\rangle$ and $\{11\bar{2}2\}\langle 11\bar{2}\bar{3}\rangle$ in various rolled and annealed AZ31 Mg alloys when the loading direction is parallel to ED and TD are shown in Fig. 11. The average Schmid factor (SF) values for $\{0001\}\langle 11\bar{2}0\rangle$ basal slip are 0.237, 0.214, 0.243, 0.264, 0.272 and 0.299 in as-received sample, A1, A2, B2, A4 and B4, respectively. The SF decreases after the first pass of Step I rolling and increases gradually as the thermal rolling process continues. It expresses an opposite trend on slip systems of $\{10\bar{1}0\}\langle 11\bar{2}0\rangle$, $\{10\bar{1}1\}\langle 11\bar{2}0\rangle$ and $\{11\bar{2}2\}\langle 11\bar{2}\bar{3}\rangle$ in various rolled Mg sheet samples. When the loading direction is parallel to TD, $\{0001\}\langle 11\bar{2}0\rangle$ basal slips are not favored; however, the average SF values increase on slip systems of $\{10\bar{1}0\}\langle 11\bar{2}0\rangle$, $\{10\bar{1}1\}\langle 11\bar{2}0\rangle$ and $\{11\bar{2}2\}\langle 11\bar{2}\bar{3}\rangle$, which is much more favored. The changing trend of SF is mainly related to the texture evolution. As shown in Figs. 4 and 10, the basal pole is much more emanative towards RD, and the intensity is reduced gradually as the two-step rolling passes increase. Due to the weakening of {0002} basal texture and rotation of grains to RD, the $\{0001\}\langle 11\bar{2}0\rangle$ basal slips are activated easily, which leads to the increased $\{0002\}\langle 11\bar{2}0\rangle$ SF when the loading direction is parallel to RD. However, the intensity of the basal texture is enhanced in the 1 pass rolled A1 sample; thus, the SF is slightly decreased. The basal slips are slightly not favored owing to the RD-tilted grain crystal, which is a hard orientation for the $\{0001\}\langle 11\bar{2}0\rangle$ basal slips when the loading direction is along TD. The more the tilted grains there are, the less favored the basal slips will be along TD. The change in SF affects the mechanical properties significantly during subsequent deformation.

3.3 Mechanical properties and anisotropy

The true tensile stress vs strain curves of various rolled and annealed AZ31 Mg alloy sheets along RD, 45° and TD are shown in Fig. 12. The mechanical properties (yield strength (YS), ultimate tensile strength (UTS), and fracture elongation (FE)

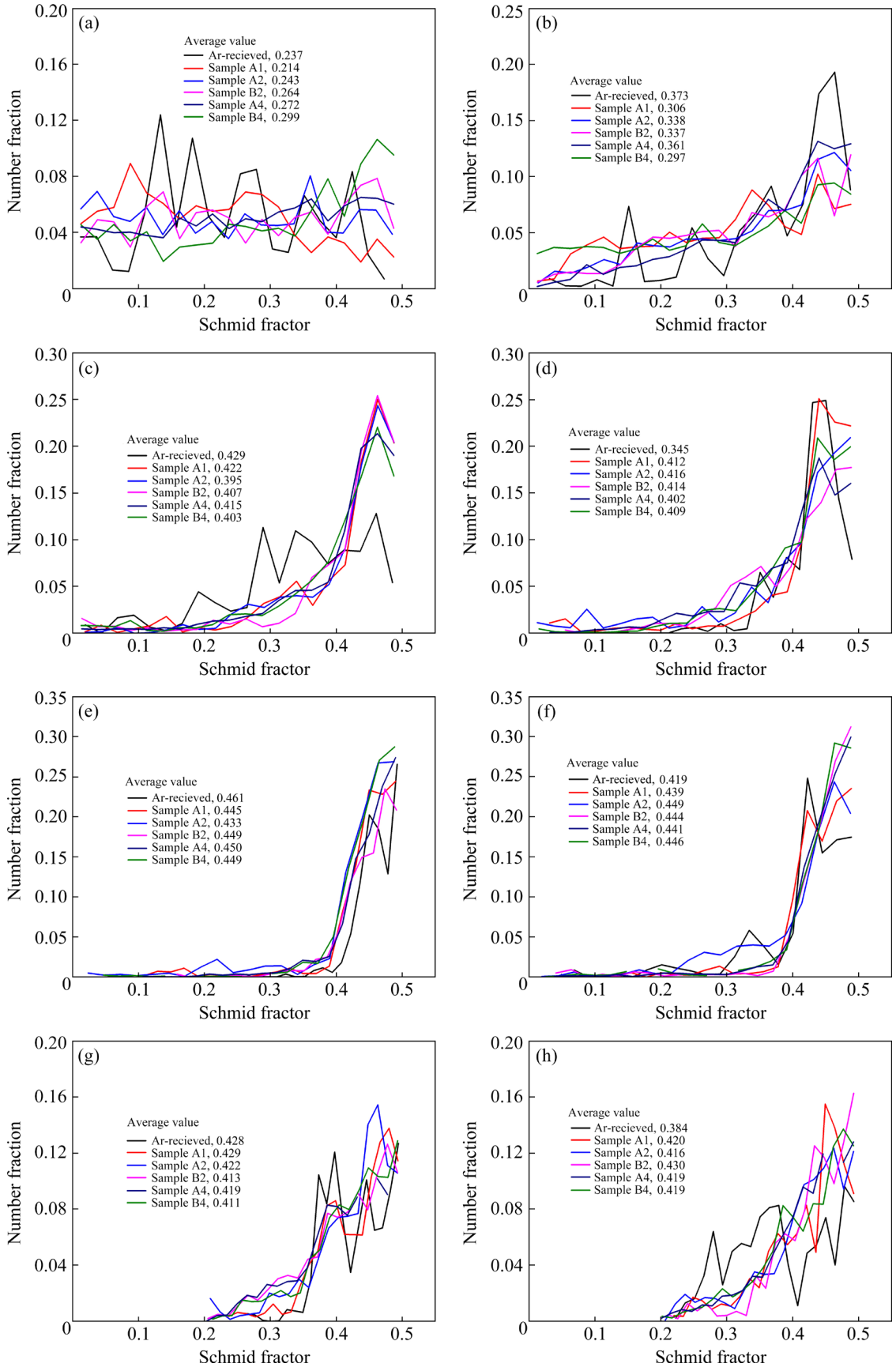

Fig. 11 Schmid factor distributions with loading axis parallel to RD (a, c, e, g) and TD (b, d, f, h) of various rolled AZ31 Mg alloys for different slip systems: (a, b) $(0002)\langle 11\bar{2}0\rangle$; (c, d) $(10\bar{1}0)\langle 11\bar{2}0\rangle$; (e, f) $\{10\bar{1}1\}\langle 11\bar{2}0\rangle$; (g, h) $\{11\bar{2}2\}\langle 11\bar{2}3\rangle$

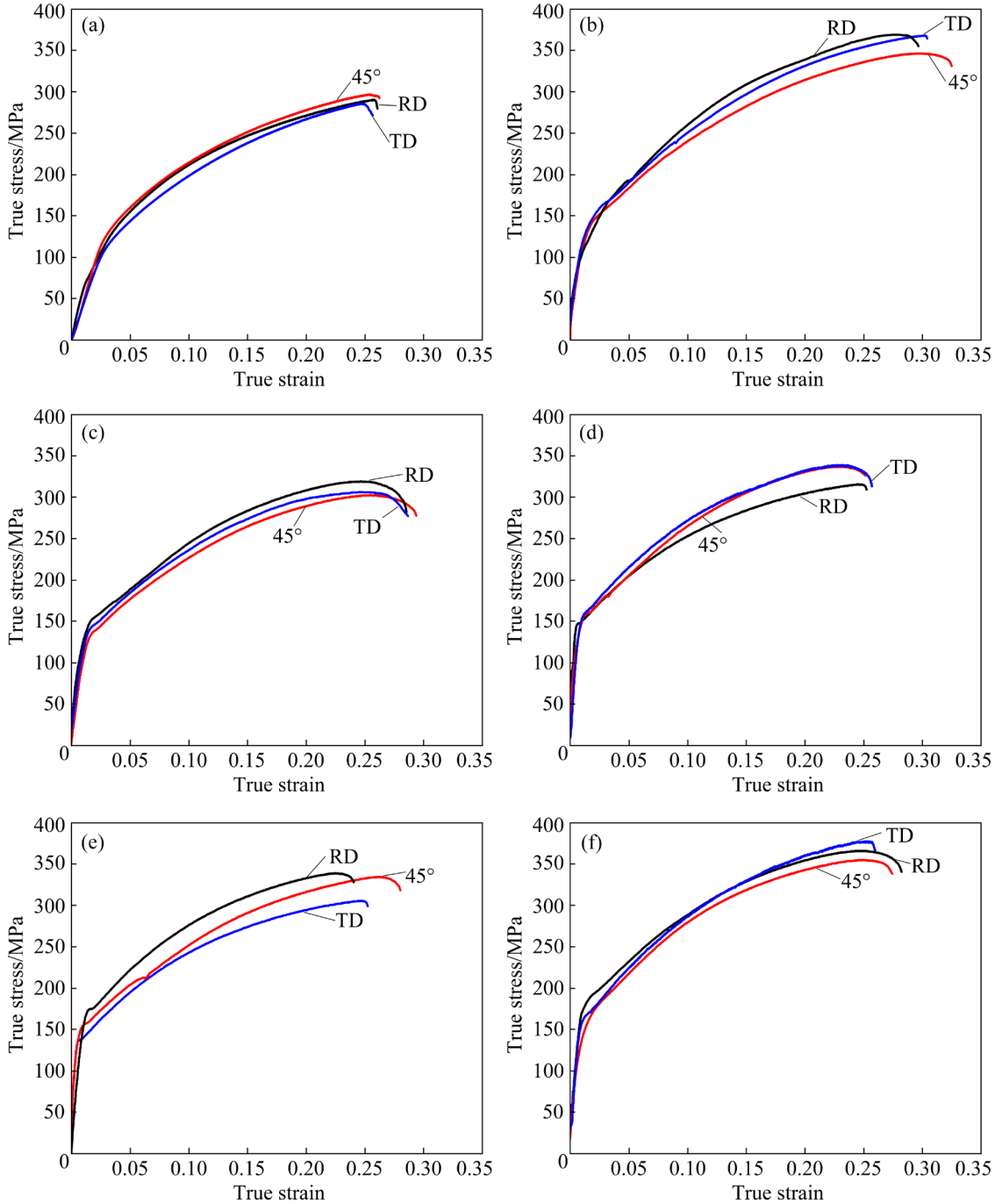

Fig. 12 True tensile stress–strain curves of various annealed AZ31 Mg alloy sheets along three directions (RD, 45° and TD): (a) As-received; (b) Sample A1; (c) Sample A2; (d) Sample B2; (e) Sample A4; (f) Sample B4

of 4-pass thermally-rolled samples are shown in Fig. 13. The flow stresses of various samples are improved after thermal rolling compared with those of as-received sample. This is mainly related to the grain refinement as well as the texture evolution. Due to fine grains, the strength is enhanced, including the yield strength and ultimate tensile strength, while the ductility is improved owing tothe promotion of basal slips induced by basal texture weakening. After Step II rolling, the basal texture is emanative to RD or TD and a tilted texture component is generated which is beneficial to the activation of basal $\langle a \rangle$ slips during the deformation in two routes of rolled samples. Especially for Samples A4 and B4 with a final thickness of 1.0 mm, the YS values of the two samples are 165.5 and 174.1 MPa, and the UTS values are 360.6 and 365.9 MPa, respectively, when

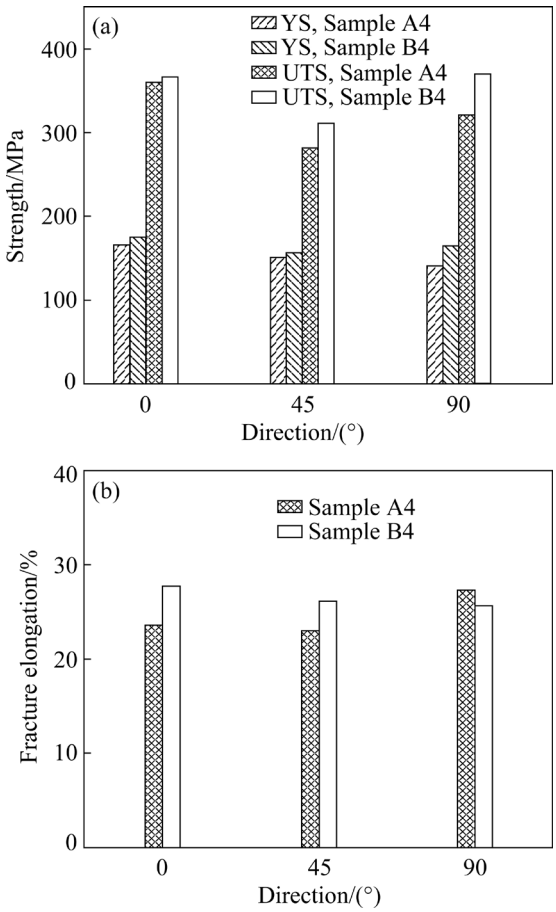

Fig. 13 Mechanical properties of 4-pass rolled AZ31 Mg sheet samples along three directions (RD, 45°, TD): (a) Yield strength (YS) and ultimate tensile strength (UTS); (b) Fracture elongation

the tensile direction is parallel to RD. Along TD, the YS values are 140.6 and 164.8 MPa, while UTS values are 318.9 and 370.1 MPa, respectively. Both the YS and UTS of Sample B4 in different directions are larger than those of Sample A4. This is because much finer grains are obtained after alternatively-changing direction rolling than unidirectional rolling.

Moreover, the differences of YS between RD and TD of Samples A4 and B4 are approximately 24.9 and 9.3 MPa, respectively. The anisotropy of YS is reduced obviously in Sample B4. The trend is similar to the sample after two passes of rolling in Samples A2 and B2. In general, a strong YS anisotropy is generated on Mg alloy sheets after multi-pass rolling owing to the basal texture [38]. The more the rolling passes and the larger the strain are, the stronger the basal texture and the anisotropy will be [39]. However, in this study, Step II rolling is carried out at higher temperature, and prismatic $\langle a \rangle$ and pyramidal $\langle a+c \rangle$ slips are promoted, which results in competition with basal $\langle a \rangle$ slips during deformation. The larger the strain levels are, the more the activation of non-basal slip is and the weaker the basal texture is, especially the generation of non-basal slip texture. From Figs. 10(d, e), the basal texture of Sample B4 is much more emanative towards RD and TD, while it tilts along RD in Sample A4. Thus, a weaker basal texture component is generated in Sample B4. ZHANG and CHENG [40] suggested that the basal texture contributed to the anisotropy of Mg alloy sheets. Therefore, the difference of YS is reduced at the same time, and the anisotropy is weakened. There is a similar reason for the fracture elongation. The increased SF of basal slips results in the larger improvement of the fracture elongation in Sample B4 compared with A4.

The strain hardening coefficient value (*n*-value) and Lankford value (*r*-value) of Samples A4 and B4 are given in Table 2. A larger average *n*-value and lower *r*-value are obtained in Sample B4 compared with Sample A4. AGNEW and DUYGULU [41], and SONG et al [6] indicated that the *n*-value and *r*-value were sensitive to the texture. With a weakened and emanative basal texture, basal slips are promoted much more obviously so that more dislocations are sustained, which results in a higher *n*-value. A larger *n*-value benefits uniform deformation, and increased fracture elongation is achieved, as shown in Fig. 13(b). The *r*-value represents the ability to prevent thickness thinning under in-plane deformation. SONG et al [42] reported that the strain along width direction was

Table 2 Strain hardening coefficient value (*n*-value) and Lankford value (*r*-value) of Samples A4 and B4 under annealed conditions

Sample	*n*-value			$\overline{n}$	*r*-value			$\overline{r}$
	RD	45°	TD		RD	45°	TD	
A4	0.2105	0.2343	0.3448	0.2559	2.126	2.273	2.968	2.410
B4	0.2972	0.2936	0.3884	0.3181	1.342	1.518	2.172	1.638

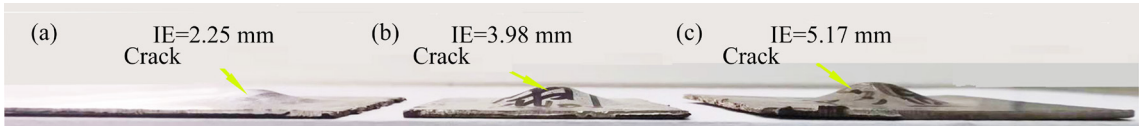

Fig. 14 Erichsen test (IE) values of various thermally-rolled AZ31 alloy sheets under annealed conditions: (a) Conventionally hot-rolled sample; (b) Sample A4; (c) Sample B4

accommodated by prismatic slips, while the strain along thickness direction was generated by pyramidal ⟨*c*+*a*⟩ slips and contraction twinning under in-plane deformation on Mg alloys. However, due to the higher CRSS of pyramidal ⟨*c*+*a*⟩ slips and contraction twinning, they are not easy to activate at room temperature; thus, a higher *r*-value is obtained. Under this condition, basal slips may play an important role in coordinating the deformation along the thickness with a weakened basal texture. In Sample A4, a tilted RD basal texture is generated after annealing so that basal slips are promoted and a higher SF is obtained when loading direction is along RD. Therefore, the strain along thickness direction is coordinated more by basal slips, which results in a smaller *r*-value. However, it increases when the loading direction is changed. In Sample B4, the basal texture is much more emanative, and grains tilt toward both RD and TD, as shown in Fig. 10(e). Thus, basal slips are enhanced along not only RD but also TD. A lower *r*-value is achieved in Sample B4. A higher *n*-value and smaller *r*-value contribute to the improvement of the stretch formability of Mg alloy sheets.

The Erichsen test (IE) values of two-step thermally-rolled Mg alloy sheet samples, A4 and B4, as well as conventionally hot-rolled (CTR) AZ31 sheets under annealed condition at room temperature are shown in Fig. 14. In order to compare the effect of two-step rolling on the formability of Mg alloys, the Erichsen test on CTR samples were conducted specially. The IE values of CTR, A4 and B4 samples are 2.25, 3.98 and 5.17 mm, respectively. Compared with the CTR sheet, the stretch formability is improved by 76.8% and 129.7% on Samples A4 and B4, respectively. Both the unidirectional and alternatively-changed-directional rolled samples during two-step increased-temperature thermal rolling express a higher formability. In addition, ZHANG et al [11] indicated that the IE values after unidirection rolling and cross-rolled samples were 3.74 and 4.81 mm on one-step rolling at 300 °C, respectively. This means that the two-step thermal rolling process has more advantages than conventional or cross rolling to enhance the formability of Mg alloy sheets independently. However, in the present study, a weakened basal texture is generated in both two-step rolled samples. Due to the weakened basal texture, the orientation of grains favors basal slips even though the deformation is along the thickness direction. Thus, the strain along thickness direction can be generated by basal slips, which benefits the coordination of the in-plane deformation. A higher *n*-value bears more work hardening so that the stress concentration is retarded and earlier failure is prevented. In addition, the smaller *r*-value provides a good capability of Mg alloy on sheet thinning, which is helpful to improving the stretch formability. Therefore, a higher IE value is obtained. Above all, the two-step thermal rolling processes have a significant effect on weakening the basal texture, especially changing the rolling routes at higher temperature.

4 Conclusions

(1) Large amounts of shear bands emerge in the microstructure of Route A rolled Mg alloy sheets; while no shear bands appear during Route B thermal rolling. This is mainly related to the promotion of DRX and non-basal slips induced by the alternatively-changing tensile and compressive stresses.

(2) Due to the competition of non-basal slips with basal slips, the basal texture is weakened on both thermally-rolled samples, and especially in Sample B4, a slightly RD-tilted non-basal texture is generated. Due to the weakening of basal texture, the anisotropy of AZ31 Mg alloy sheets is reduced, and the difference of YS between RD and TD on Sample B4 is only 9.3 MPa. A higher *n*-value and smaller *r*-value are achieved.

(3) IE values of the final AZ31 Mg alloy sheets after four-pass rolled samples, A4 and B4, are 3.98 and 5.17 mm, respectively, which are

higher than those of conventionally rolled sheets. The weakened basal texture results in more improvement by 29.9% on Sample B4 than on Sample A4. Two-step increased-temperature direction changing thermal rolling is proven to be a more effective method to enhance the stretch formability of AZ31 Mg alloy sheets.

Acknowledgments

The authors thank the National Natural Science Foundation of China (Nos. 51704209, U1810208, U1810122), the Central Government Guided Local Science and Technology Development Projects, China (No. YDZJSX-2021A010), the Projects of International Cooperation in Shanxi Province, China (Nos. 201803D421086, 201903D421076), Shanxi Province Patent Promotion Implementation Fund, China (No. 20200718), the Technological Innovation Programs of Higher Education Institutions in Shanxi Province, China (No. 201802034), Shanxi Province Scientific Facilities and Instruments Shared Service Platform of Magnesium-based Materials Electric Impulse Aided Forming, China (No. 201805D141005), Science and Technology Major Project of Shanxi Province, China (Nos. 20191102008, 20191102007, 20181101008), and Yantai High-end Talent Introduction “Double Hundred Plan”, China (2021).

References

[1] TIAN Yuan, MIAO Hong-wei, NIU Jia-lin, HUANG Hua, KANG Ga-bin, ZENG Hui, DING Wen-jiang, YUAN Guang-yin. Effects of annealing on mechanical properties and degradation behavior of biodegradable JDBM magnesium alloy wires [J]. Transactions of Nonferrous Metals Society of China, 2021, 31: 2615−2625.

[2] AHMADI S, ALIMIRZALOO V, FARAJI G, DONIAVI A. Properties inhomogeneity of AM60 magnesium alloy processed by cyclic extrusion compression angular pressing followed by extrusion [J]. Transactions of Nonferrous Metals Society of China, 2021, 31: 655−665.

[3] LUO Xian, TAN Qi-yang, MO Ning, YIN Yu, YANG Yan-qing, ZHUANG Wyman, ZHANG Ming-xing. Effect of deep surface rolling on microstructure and properties of AZ91 magnesium alloy [J]. Transactions of Nonferrous Metals Society of China, 2019, 29: 1424−1429.

[4] ZHAO Hong-liang, HUA Yun-xiao, DONG Xiang-lei, XING Hui, LU Yan-li. Influence of trace Ca addition on texture and stretch formability of AM50 magnesium alloy sheet [J]. Transactions of Nonferrous Metals Society of China, 2020, 30: 647−656.

[5] ZHANG Hua, HUANG Guang-sheng, KONG De-qiang, SANG Gao-feng, SONG Bo. Influence of initial texture on formability of AZ31B magnesium alloy sheets at different temperatures [J]. Journal of Materials Processing Technology, 2011, 211: 1575−1580.

[6] SONG Deng-hui, ZHOU Tao, TU Jian, SHI Lai-xin, Song Bo, HU Li, YANG Ming-bo, CHEN Qiang, LU Li-wei. Improved stretch formability of AZ31 sheet via texture control by introducing a continuous bending channel into equal channel angular rolling [J]. Journal of Materials Processing Technology, 2018, 259: 380−386.

[7] CHINO Y, KADO M, MABUCHI M. Enhancement of tensile ductility and stretch formability of magnesium by addition of 0.2 wt.% (0.035 at.%) Ce [J]. Materials Science and Engineering A, 2008, 494: 343−349.

[8] CHAUDRY U M, KIM Y S, HAMAD K. Effect of Ca addition on the room-temperature formability of AZ31 magnesium alloy [J]. Materials Letters, 2019, 238: 305−308.

[9] TROJANOVÁ Z, KRAL R, CHATEY A. Deformation behavior of an AJ50 magnesium alloy at elevated temperatures [J]. Materials Science and Engineering A, 2007, 462: 202−205.

[10] HUANG Xin-sheng, SUZUKI K, CHINO Y, MABUCHI M. Improvement of stretch formability of Mg−3Al−1Zn Alloy sheet by high temperature rolling at finishing pass [J]. Journal of Alloys and Compounds, 2011, 509: 7579−7584.

[11] ZHANG Hua, HUANG Guang-sheng, ROVEN H J, WANG Li-fei, PAN Fu-sheng. Influence of different rolling routes on the microstructure evolution and properties of AZ31 Magnesium alloy sheets [J]. Materials & Design, 2013, 50: 667−673.

[12] MA Ru, LU Yue, WANG Ling, WANG Yi-nong. Influence of rolling route on microstructure and mechanical properties of AZ31 magnesium alloy during asymmetric reduction rolling [J]. Transactions of Nonferrous Metals Society of China, 2018, 28: 902−911.

[13] KUANG Jie, ZHANG Yu-qing, DU Xin-peng, ZHANG Jin-yu, LIU Gang, SUN Jun. On the strengthening and slip activity of Mg−3Al−1Zn alloy with pre-Induced $\{10\bar{1}2\}$ twins [J]. Journal of Magnesium and Alloys, 2021, https://doi.org/10.1016/j.jma.2021.07.016.

[14] LI Na, YAMG Ling-wei, WANG Chuan-yun, MONCLÚS M A, MOLINA-ALDAREGUÍA J M. Deformation mechanisms of basal slip, twinning and non-basal slips in Mg−Y alloy by micropillar compression [J]. Materials Science and Engineering A, 2021, 819: 141408.

[15] ZHI Chen-chen, MA Li-feng, HUANG Qing-xue, HUANG Zhi-quan, LIN Jin-bao. Improvement of magnesium alloy edge cracks by multi-cross rolling [J]. Journal of Materials Processing Technology, 2017, 255: 333−339.

[16] GUO Fei, ZHANG Ding-fei, YANG Xu-sheng, JIANG Lu-yao, Pan Fu-sheng. Microstructure and texture evolution of AZ31 magnesium alloy during large strain hot rolling [J]. Transactions of Nonferrous Metals Society of China, 2015, 25: 14−21.

[17] CHUN Y B, DAVIES H J. Investigation of prism a slip in warm-rolled AZ31 alloy [J]. Metallurgical and Materials Transactions A, 2011, 42: 4113−4125.

[18] CHUN Y B, BATTAINI M, DAVIES C H J, WANG S K. Distribution characteristics of in-grain misorientation axes in cold-rolled commercially pure titanium and their correlation with active slip modes [J]. Metallurgical and Materials Transactions A, 2010, 41: 3473−3487.

[19] HAGIHARA K, FUKUSUMI Y, YAMASAKI M, NAKNO T, KAWAMURA Y. Non-basal slip systems operative in $Mg_{12}ZnY$ long-period stacking ordered (LPSO) phase with 18R and 14H structures [J]. Materials Transactions, 2013, 54: 693−697.

[20] TAKAGI K, YAMASAKI M, MINE Y, TAKASHIMA K. Temperature dependence of prismatic slip in a single-crystalline long-period stacking ordered Mg−Zn−Y alloy [J]. Scripta Materialia, 2020, 178: 498−502.

[21] HAPUIS A C, DRIVER J H. Temperature dependency of slip and twinning in plane strain compressed magnesium single crystals [J]. Acta Materialia, 2011, 59: 1986−1994.

[22] LIAO Juan, ZHANG Li-xia, XIANG Hong-liang, XUE Xin. Mechanical behavior and microstructure evolution of AZ31 magnesium alloy sheet in an ultrasonic vibration-assisted hot tensile test [J]. Journal of Alloys and Compounds, 2021, 895: 162575.

[23] CHO J H, KIM H W, KANG S B, HAN T S. Bending behavior, and evolution of texture and microstructure during differential speed warm rolling of AZ31B magnesium alloys [J]. Acta Materialia, 2011, 59: 5638−5651.

[24] ZHANG Kai, ZHANG Jing-hua, HUANG Yan, PRUNCU C, JIANG Jun. Evolution of twinning and shear bands in magnesium alloys during rolling at room and cryogenic temperature [J]. Materials & Design, 2020, 193: 108793.

[25] JIA Wei-tao, MA Li-feng, TANG Yan, LE Qi-chi, FU Li. Relationship between microstructure and properties during multi-pass, variable routes and different initial temperatures hot flat rolling of AZ31B magnesium alloy [J]. Materials & Design, 2016, 103: 171−182.

[26] BASU I, SAMMAN A T, GOTTSTEIN G. Shear band-related recrystallization and grain growth in two rolled magnesium-rare earth alloys [J]. Materials Science and Engineering A, 2013, 579: 50−56.

[27] GUAN Di-kai, RAINFORTH W M, LE Ma, WYNNE B, GAO Jun-heng. Twin recrystallization mechanisms and exceptional contribution to texture evolution during annealing in a magnesium Alloy [J]. Acta Materialia, 2017, 126: 132−144.

[28] GUAN Lei, TANG Guo-yi, JIANG Yan-bin, CHU P K. Texture evolution in cold-rolled AZ31 magnesium alloy during electropulsing treatment [J]. Journal of Alloys and Compounds, 2009, 487: 309−313.

[29] SAMMAN A T, GOTTSTEIN G. Room Temperature formability of a magnesium AZ31 alloy: Examining the role of texture on the deformation mechanisms [J]. Materials Science and Engineering A, 2008, 488: 406−414.

[30] SU Jing, KABIR A S H, SANJARI M, YUE S. Correlation of static recrystallization and texture weakening of AZ31 magnesium alloy sheets subjected to high speed rolling [J]. Materials Science and Engineering A, 2016, 674: 343−360.

[31] ZENG Zuo-ran, ZHU Yu-man, XU S W, BIAN M Z, DAVUES C H J, BIRBILIS N, NIE Jian-feng. Texture evolution during static recrystallization of cold-rolled magnesium alloys [J]. Acta Materialia, 2016, 105: 479−494.

[32] HUANG Xin-sheng, SUZUKI K, CHINO Y, MABUCHI M. Influence of rolling temperature on static recrystallization behavior of AZ31 magnesium alloy [J]. Journal of Materials Science, 2012, 47: 4561−4567.

[33] FLYNN P W, MOTE J, DORN J E. On the Thermally activated mechanism of prismatic slip in magnesium single crystals [M]. University of California, Berkeley, 1961.

[34] PRASAD Y V R K, RAO K P. Effect of Crystallographic texture on the kinetics of hot deformation of rolled Mg−3Al−1Zn alloy plate [J]. Materials Science and Engineering A, 2006, 432: 170−177.

[35] HUANG Xin-sheng, SUZUKI K, SAITO N. Textures and stretch formability of Mg−6Al−1Zn magnesium alloy sheets rolled at high temperatures up to 793 K [J]. Scripta Materialia, 2009, 60: 651−654.

[36] HUANG Xin-sheng, SUZUKI K, CHINO Y. Influences of initial texture on microstructure and stretch formability of Mg–3Al–1Zn Alloy sheet obtained by a combination of high temperature and subsequent warm rolling [J]. Scripta Materialia, 2010, 63: 395−398.

[37] ZHANG Hua, HUANG Guang-sheng, WANG Li-fei, ROVEN H J, PAN Fu-sheng. Enhanced mechanical properties of AZ31 magnesium alloy sheets processed by three-directional rolling [J]. Journal of Alloys and Compounds, 2013, 575: 408−413.

[38] YAO Yi, LIU Chu-ming, WAN Ying-chun, YU Shi-lun, GAO Yong-hao, JIANG Shun-nong. Microstructure, texture and mechanical anisotropy of Mg−Gd−Y−Zr sheets processed via different rolling routes and reductions [J]. Materials Characterization, 2020, 161: 110120.

[39] LIU Di, LIU Zu-yan, WANG Er-de. Effect of rolling reduction on microstructure, texture, mechanical properties and mechanical anisotropy of AZ31 magnesium alloys [J]. Materials Science and Engineering A, 2014, 612: 208−213.

[40] ZHANG Xiao-hua, CHENG Yuan-sheng. Tensile anisotropy of AZ91 magnesium alloy by equal channel angular processing [J]. Journal of Alloys and Compounds, 2015, 622: 1105−1109.

[41] AGNEW S R, DUYGULU O. Plastic anisotropy and the role of non-basal slip in magnesium alloy AZ31B [J]. International Journal of Plasticity, 2005, 21: 1161−1193.

[42] SONG Bo, GUO Ning, LIU Ting-ting, YANG Qing-shan. Improvement of formability and mechanical properties of magnesium alloys via pre-twinning: A review [J]. Materials & Design, 2014, 62: 352−360.

两步升温热轧工艺对 AZ31 镁合金薄板各向异性及成形性能影响

王利飞[1,2,3]，潘晓锾[1]，朱星晓[1]，邢 镔[2]，张 华[4]，
卢立伟[5]，王红霞[1]，程伟丽[1]，Maurizio VEDANI[6]

1. 太原理工大学 材料科学与工程学院 先进镁基材料山西省重点实验室，太原 030024；
2. 重庆工业大数据创新中心有限公司 工业大数据应用技术国家工程实验室，重庆 400707；
3. 上海交通大学 材料科学与工程学院，上海 200240；
4. 烟台大学 精准材料高等研究院，烟台 264005；
5. 湖南科技大学 难加工材料高效精密加工湖南省重点实验室，湘潭 411201；
6. Department of Mechanical Engineering, Politecnico di Milano, 20156 Milan, Italy

摘 要：采用两步梯度升温轧制工艺对 AZ31 镁合金板材进行轧制，探究轧制过程对镁合金板材显微组织织演化、各向异性及成形性能的影响。第 I 步轧制在 300 ℃开展，其每道次压下量为 15%；第 II 步轧制在 550 ℃进行，其每道次压下量为 40%。经过共 4 道次轧制后，最终获得厚度为 1 mm 的镁合金薄板。结果显示，第 I 步低温轧制过程不更换轧制方向时，试样中生成大量剪切带；而更换轧制方向时，组织内部主要为孪晶和再结晶晶粒。随着 II 步轧制温度的升高，由于动态再结晶急剧激发，剪切带数量及尺寸逐渐减小，晶粒明显细化。根据 IGMA 分析得出，非基面滑移，特别是棱柱面⟨*a*⟩滑移活动增强。轧制退火后的 AZ31 镁合金薄板的力学性能得到提高，各向异性减小，冲压成形性能得到明显改善。

关键词：镁合金板材；两步升温热轧；非基面滑移；剪切带；织构；成形性能

(Edited by Bing YANG)